



In vivo time-course biocompatibility assessment of biomagnetic nanoparticles-based biomaterials for tissue engineering applications

Fernando Campos, Ana Belén Bonhome-Espinosa, Carmona Ramón, Juan D.G. Durán, Pavel Kuzhir, Miguel Alaminos, Modesto Lopez-Lopez, Ismael Rodriguez, Victor Carriel

► To cite this version:

Fernando Campos, Ana Belén Bonhome-Espinosa, Carmona Ramón, Juan D.G. Durán, Pavel Kuzhir, et al.. In vivo time-course biocompatibility assessment of biomagnetic nanoparticles-based biomaterials for tissue engineering applications. *Materials Science and Engineering: C*, 2021, 118, pp.111476. 10.1016/j.msec.2020.111476 . hal-03088294

HAL Id: hal-03088294

<https://hal.science/hal-03088294>

Submitted on 19 Jan 2021

HAL is a multi-disciplinary open access archive for the deposit and dissemination of scientific research documents, whether they are published or not. The documents may come from teaching and research institutions in France or abroad, or from public or private research centers.

L'archive ouverte pluridisciplinaire **HAL**, est destinée au dépôt et à la diffusion de documents scientifiques de niveau recherche, publiés ou non, émanant des établissements d'enseignement et de recherche français ou étrangers, des laboratoires publics ou privés.

***In vivo* time-course biocompatibility assessment of biomagnetic nanoparticles-based biomaterials for tissue engineering applications**

Fernando Campos^{1,5}, Ana Belén Bonhome-Espinosa³, Ramón Carmona⁴, Juan de Dios García López-Durán^{3,5}, Pavel Kuzhir⁶, Miguel Alaminos^{1,5}, Modesto Torcuato López-López^{3,5*}, Ismael Angel Rodriguez^{1,2,a*}, Víctor Carriel^{1,5,a}

¹-Department of Histology, Tissue Engineering Group, Faculty of Medicine, University of Granada, Granada, Spain.

²-Department of Histology, Faculty of Dentistry, Nacional University of Cordoba, Cordoba, Argentina.

³-Department of Applied Physics, University of Granada, Avenida de la Fuente Nueva, 18071 Granada, Spain.

⁴-Department of Cell Biology, Faculty of Sciences, University of Granada, Campus Fuentenueva s/n, Granada, Spain.

⁵-Instituto de Investigación Biosanitaria ibs.GRANADA, Granada, Spain.

⁶-University Côte d'Azur, CNRS UMR 7010, Institute of Physics of Nice, Parc Valrose, 06108, Nice, Cedex2, France.

^a These authors contributed equally: Víctor Carriel, Ismael Angel Rodriguez.

* Corresponding: Prof. Dr. Modesto Torcuato López-López & Prof. Dr. Ismael Rodriguez, Department of Applied Physics and Department of Histology, Tissue Engineering Group, University of Granada, Granada, Spain. Email: modesto@ugr.es; ismael.rodriguez@unc.edu.ar

Abstract:

Novel artificial tissues with potential usefulness in local-based therapies have been generated by tissue engineering using magnetic-responsive nanoparticles (MNPs). In this study, we performed a comprehensive *in vivo* characterization of bioengineered magnetic fibrin-agarose tissue-like biomaterials. First, *in vitro* analyses were performed and the cytocompatibility of MNPs was demonstrated. Then, bioartificial tissues were generated and subcutaneously implanted in Wistar rats and their biodistribution, biocompatibility and functionality were analysed at the morphological, histological, haematological and biochemical levels as compared to injected MNPs. Magnetic Resonance Image (MRI), histology and magnetometry confirmed the presence of MNPs restricted to the grafting area after 12 weeks. Histologically, we found a local initial inflammatory response that decreased with time. Structural, ultrastructural, haematological and biochemical analyses of vital organs showed absence of damage or failure. This study demonstrated that the novel magnetic tissue-like biomaterials with improved biomechanical properties fulfil the biosafety and biocompatibility requirements for future clinical use and support the use of these biomaterials as an alternative delivery route for magnetic nanoparticles.

Key words: Tissue Engineering, Magnetic nanoparticles, Biomaterials, Bio-distribution, *In vivo* biocompatibility

1. Introduction

During the last years, magnetic nanoparticles (MNPs) have been evaluated in biomedicine for hyperthermia induction [1], cell labelling and separation [2], DNA separation [3], magnetic resonance imaging [4] and for drug or gene therapies [5, 6]. Iron oxide MNPs are the most commonly used, especially Fe_3O_4 (magnetite) and $\gamma\text{-Fe}_2\text{O}_3$ (maghemite), because these are stable from a thermal, chemical and colloidal standpoint. In addition, based on the MNPs magnetic properties, it was hypothesized that these particles could be guided to specific *in vivo* locations using a magnetic field gradient. This could be useful as an alternative method to concentrate growth factors, drugs or cells associated to the particles [7-9], and it has been postulated that MNPs could be useful tools for theranostic [10] and local-based tissue engineering applications [11-15]. MNPs were previously tested for the generation of bioengineered magnetic tissue-like substitutes with improved properties without affecting cell adhesion, proliferation, viability or differentiation *in vitro* [16, 17], showing a significant improvement of the biomechanical properties of these biomaterials [13, 17].

Concerning the *in vivo* biodistribution of MNPs, it is clear that the administration route is a critical factor determining bioavailability and *in vivo* functionality of MNPs [10]. To the date, several studies focused on determining the fate of these particles when injected into the bloodstream [10] and results demonstrated that injected MNPs have a short lifespan, tend to accumulate in different organs and may have a certain degree of cytotoxic effects [10, 18]. However, the *in vivo* biodistribution of particles used within biomaterials needs further characterization [14], and *in vivo* studies evaluating the cellular and molecular processes related to biocompatibility, biodegradability and biodistribution of implanted magnetic hydrogels are in need. Our group previously developed a fibrin-agarose hydrogel (FAH), which was successfully used in numerous tissue engineering applications [19-26] and is currently used in clinical trials with the approval of the Spanish Agency of Medicines and Medical Devices (AEMPS) according to the EU guidelines for clinical use [27]. Therefore, FAH can be a useful carrier candidate to be combined with MNPs in order to generate novel biocompatible magnetic tissue-like biomaterials [12, 13, 17].

The aim of this study is to determine the biocompatibility of FAH-based magnetic tissue-like biomaterials containing MagNP-OH magnetic nanoparticles and to study their *in vivo* biodistribution in a rat model. First, the structure and biocompatibility of the magnetic hydrogels were determined *in vitro*. Then, magnetic scaffolds and scaffold-free MNPs were subcutaneously grafted in animals and the host response was evaluated by magnetic resonance imaging, laboratory testing, histology and magnetometry after 12 weeks *in vivo*.

2. Materials and methods

2.1 *In vitro* analyses

2.1.1 Magnetic nanoparticles (MNPs) characterization

In this study, we used commercially available MNPs (Nanomyp, Granada, Spain) referred to as MagNP-OH. These MNPs are composed by a polycrystalline magnetite core coated with methyl methacrylate-co-hydroxyl ethyl methacrylate-co-ethylene glycol dimethacrylate (MMA-co-HEMA-co-EGDMA). The MagNP-OH particles were prepared for analyses following previously described procedures [13, 17].

The ultrastructure and dimensions of the MagNP-OH were determined by using a LIBRA 120 PLUS Carl Zeiss (Carl Zeiss, Oberkochen, Germany) transmission electron microscope (TEM). The magnetic properties of the MagNP-OH were characterized by a vibrating sample magnetometer VSM 4500 (EG&G Princeton Applied Research, NJ).

2.1.2 Analysis of biocompatibility of the MagNP-OH on 2D cell cultures

2.1.2.1 Cell culture and cell-MagNP-OH interaction model

Human fibroblast, primary cultures obtained from human oral mucosa biopsies were cultured for 24 h in 24-well plates (2×10^4 cells/well) with Dulbecco's Modified Eagle Medium (DMEM) with 10 % Fetal Bovine Serum (FBS) and antibiotics/antimycotics commercial cocktail solution (all cell culture reagents from Sigma-Aldrich, Steinheim, Germany) at 37°C with 5% of CO₂. MagNP-OH particles were added to cultured cells at a concentration of 0.5% and 1% (w/v) in DMEM (without FBS and antibiotics) and were kept in culture for 24 h, and biocompatibility was determined after this time. As positive controls of live cells (100% cell viability), the same cells were cultured without MagNP-OH particles. As negative controls (100% cytotoxicity), cells were incubated in the same medium with 1% of triton X-100 (PanReac AppliChem, Barcelona, Spain). Biocompatibility was analysed in six independent samples and viability was evaluated 4 times in each sample (24 measures per test and condition).

2.1.2.2 In vitro assessment of MagNP-OH cytocompatibility

Cytocompatibility was evaluated using a combination of morphological analyses, functional WST-1 cell viability/proliferation assay and quantification of free DNA released from dead cells (able to detect cell membrane structural integrity), as previously described [20, 28, 29]. First, the morphological changes associated with the presence of MagNP-OH were determined by phase contrast microscopy. Then, we analysed the metabolic activity of the human cells using commercially available WST-1 assays (Roche Diagnostic, Mannheim, Germany) using a Microplate Reader (Biochrom® Asys UVM340, Cambridge, UK) at a wavelength of 450–690 nm [20, 28]. Finally, the DNA-released as a consequence of irreversible cell membrane damage was quantified by using a NanoDrop 2000 UV-vis spectrophotometer (Thermo Fisher Scientific, Waltham, MA, USA) [14, 20].

2.1.2.3 Preparation of the magnetic tissue-like biomaterials

In this study, we prepared three types of scaffolds: non-magnetic FAH, and two types of magnetic FAH: FAH containing MagNP-OH (FAH-MNPs), and FAH containing MagNP-OH with the application of a definite magnetic field during gelation (FAH-MNPs-F). For the preparation of FAH and the magnetic scaffolds (FAH-MNPs and FAH-MNPs-F), we used a variation of a previously described method for non-magnetic FAH [19, 20, 22, 29, 30]. Briefly, hydrogels were generated by mixing 70% of human plasma, 13.5% of PBS (0.1M, pH 7.2-7.4) containing or not MagNP-OH (0.5% v/v of final hydrogel volume) and 1.5% of tranexamic acid (Amchafibrin, Fides-Ecofarma, Valencia, Spain). This solution was carefully mixed and then, a 2% solution of CaCl₂ was added (10% of the final volume) to promote fibrin gelation, followed by 5% volume of melted 2% type VII agarose (both by Sigma-Aldrich, Steinheim, Germany) in PBS. This mixture was aliquoted and kept in a cell incubator using standard culture conditions until complete gelation [13]. In the case of FAH-MNPs-F, the mixture was subjected to a vertical magnetic field (48 kA/m) during the first 5 minutes of the process of jellification to obtain an anisotropic biomaterial composed by aligned fibres as previously reported [13]. The process, by which the hydrogel is formed, has been previously described [20, 22, 28]. Concisely, an addition of CaCl₂ can activate the blood coagulation factors of the human plasma, resulting in the cleavage of fibrinogen by thrombin, with the subsequent polymerization of fibrin monomers into an insoluble fibrin gel [31]. At the same time, the agarose polysaccharides jellify by forming hydrogen bonds on the fibrin fibres as temperature decreases [32, 33].

2.1.2.4 Analysis of biomechanical properties of the magnetic tissue-like biomaterials

Magnetic and non-magnetic tissue-like biomaterials were subjected to oscillatory shear strains of increasing amplitude and fixed frequency (1 Hz), and the corresponding oscillatory shear stress was assessed using a Haake MARS III (Thermo Fisher Scientific, Waltham, MA, USA) rheometer at 37°C. The measuring system geometry was a 3.5 cm diameter parallel plate set with rough surfaces to avoid wall slip, and the rotating plate was adjusted to a normal force of 5 N. Measurements were conducted under oscillatory shear strains and the biomechanical properties of the different tissue-like biomaterials were studied by determining the complex viscoelastic modulus of each sample.

2.2 In vivo analyses

2.2.1 Laboratory animals

In this study, a total of eighty-five 12-week-old adult male Wistar rats weighing 250–300 g were used. Animals were maintained in the Experimental Unit of the University Hospital Virgen de las Nieves in Granada (Spain). Animals were housed in a temperature-controlled room ($21 \pm 1^\circ\text{C}$) on a 12 h light/dark cycle with *ad libitum* access to tap water and standard rat chow. These studies were performed according to the European Union and Spanish Government guidelines for the ethical care of animals (EU Directive No. 63/2010, RD 53/2013) and this project was approved by the CEEA ethical committee for animal experimentation (approval number: 03-7-15-311).

2.2.2 Surgical procedure and experimental groups

For the *in vivo* biocompatibility evaluation of magnetic tissue-like biomaterials, and to study the biodistribution of the MagNP-OH, animals were deeply anaesthetized by intraperitoneal injection of a mixture of acepromazine (Calmo-Neosan®, 0.001 mg/g of the weight of the animal, Boehringer Ingelheim, Ingelheim am Rhein, Germany) and ketamine (Imalgene 1000®, 0.15 mg/g of the weight of the animal, Boehringer Ingelheim). Each animal was randomly assigned to one of the following experimental groups ($n = 20$ in each except for the control group):

- (i) FAH group: once anaesthetized, a 1 cm-long incision was made in the forearm skin of each animal, a FAH tissue-like substitute was subcutaneously grafted, and the injury was repaired using absorbable sutures. These animals were used as a control group.
- (ii) FAH-MNPs group: in these animals, FAH containing 0.5% (v/v) MagNP-OH were implanted following the same procedure described for the FAH group.
- (iii) FAH-MNPs-F group: FAH containing 0.5% (v/v) MagNP-OH subjected to a magnetic field during gelation were implanted.
- (iv) MNPs-INJ group: in this case, MNPs were injected in the same area of groups i, ii and iii (forearm subcutaneous tissue). In this sense, subcutaneous injection of a solution containing the MNPs was given in both forearms of each rat (250 μl of a sterile physiological solution containing 12.5 mg of MagNP-OH).
- (v) CTR group: five healthy animals were used as controls.

Animals were euthanized after 1, 3, 5 or 12 weeks ($n = 5$ in each period) by using an overdose of anaesthetics followed by intracardiac perfusion of fixative.

2.2.3 Magnetic resonance imaging (MRI)

Magnetic Resonance Image (MRI) analysis was used to identify the grafted materials in each animal and to assess the effects of these materials on the morphology of some major body organs. For this purpose, 3 animals

corresponding to each experimental group (CTR, FAH, FAH-MNPs, FAH-MNPs-F and MNPs-INJ) were analysed after 1, 3, 5, and 12 weeks of the surgical procedure using a Biospec TM 70/20 USR device equipped with 7 Tesla Ultrashield Refrigerated magnets (Bruker, Billerica, MA). This device was designed and optimized for the analysis of small experimentation animals and is available at the Scientific Research Facility of the University of Granada, Spain. First, animals were anesthetized with isoflurane using a Ohmeda veterinary anaesthesia unit and immobilized in a MRI-compatible cradle. Temperature was kept at 37°C using a water bath circulation system. Then, a whole-body scan was performed on each animal, and the morphology of liver, kidneys, lymph nodes and spleen was evaluated, and the grafting site was specifically analysed to determine the MRI morphology of the implant site and possible migration of the particles to local and regional tissues. In all cases, high resolution axial T2-weighted images were acquired through a T2-TurboRARE sequence using the following settings and experimental conditions: echo time = 23 ms; rare factor = 8 and slice thickness = 1 mm; repetition time = 1371.177 ms with average = 8.

2.2.4 Haematological and biochemical studies

1.5 mL of blood was collected from 5 animals corresponding to each experimental condition at 1, 3, 5 and 12 weeks of *in vivo* follow-up. Blood was stored in Eppendorf tubes containing 5% heparin. For complete blood count, a Sysmex KX-21N automatic analyser (Roche Laboratories, Basel, Switzerland) was used as previously described [32] to determine the following haematological parameters: concentration of haemoglobin (HGB), erythrocytes count (RCB), haematocrit count (HCT), platelets (PLT), white blood cells (WBC), lymphocytes (LYM), neutrophils (NEUT), monocytes-basophils-eosinophils (MXD) [34, 35].

For biochemical tests, blood was centrifuged for 15 min at 3,500 rpm and the supernatant serum was collected for analysis using a clinical chemistry analyser Cobas c311 (Roche Laboratories, Basel, Switzerland). The following biochemical parameters were analysed in each sample: Alanine aminotransferase (ALT), urea (UREA), creatinine (CREJ2), iron (IRON2) (all RTU kits from Roche Laboratories) [34, 35].

2.2.5 Histological and histochemical studies

For the histological analyses, animals were deeply anaesthetized and perfused with 4% neutral buffered paraformaldehyde. For all animals included in the study, the area of the implant (FAH, FAH-MNPs, FAH-MNPs-F and MNPs-INJ) was carefully dissected and post-fixed in 4% neutral buffered formaldehyde for 24 h, dehydrated and embedded in paraffin. For animals corresponding to 1 and 12 weeks of follow-up, four vital organs (liver, kidneys, lymph nodes and spleen) were also extracted, post-fixed and embedded in paraffin. Tissue blocks were sectioned at 5 µm of thickness, rehydrated and stained with haematoxylin-eosin (H&E) for histological evaluation. In addition, different histochemical techniques were used to determine tissue-specific normal parameters. The periodic acid-Schiff histochemical method (PAS) was used to evaluate the glycogen content of the liver, the glomerular basement membrane of the kidney and the basement membranes of each tissue and organ. To identify the presence of ferric iron, all tissues and organs were stained with Perls (Prussian blue reaction) histochemical method contrasted with H&E as described previously [14].

The percentage of positive area for Perls-positive histochemical reaction in the spleen was determined with ImageJ software (National Institutes of Health, USA) from each group at 1 and 12 weeks following a previously described methodology [28, 36].

2.2.6 Ultrastructural analyses

For the ultrastructural analyses, tissue samples corresponding to the 12 weeks follow-up period were obtained from each animal included in the *in vivo* study at the moment of the euthanasia. Samples were fixed in 2.5% glutaraldehyde, washed three times in cacodylate buffer and post-fixed in 1% osmium tetroxide. Tissues were then dehydrated and embedded in epoxy resin, and sectioned. Ultrathin sections were stained with aqueous uranyl acetate and lead citrate, mounted on grids and analysed in a Carl Zeiss EM902 transmission electron microscope. The presence of iron atoms in tissues was identified by Electron Energy-Loss Spectroscopy (EELS). Analysis of the heterogeneous pattern of the FAH, FAH-MNPs and FAH-MNPs-F was carried out by scanning electron microscopy (SEM) using a FEI Quanta 200 equipment (Hillsboro, OR) as previously described [20, 22, 28].

2.2.7 Magnetometry

After the euthanasia, we tracked the presence of particles at the site of implantation and vital organs. We checked the magnetic response of the samples with a neodymium magnet in a magnetic field gradient of 10 mT/mm and a maximum field of 470 mT. In addition, we quantified the magnetic response of the samples through magnetometry measurements using a vibrating sample magnetometer VSM 4500 (EG&G Princeton Applied Research, NJ) at room temperature. For this, similar volumes of tissue (equivalent to 50 mg of mass) were used from each condition. The detection limit of the magnetometer was 0.001 emu/g, which corresponds to approximately 30 μg of particles. These analyses were performed in animals corresponding to 12 weeks of *in vivo* follow-up.

2.2.8 Statistical analyses

In this study, all variables were subjected to the Shapiro-Wilk test of normality and resulted to be non-normally distributed. Therefore, Fisher Exact Test and Mann-Whitney *U* test were used to determine statistical differences between comparison groups. All variables were analysed by using the software SPSS 16.00 (IBM Company, Armonk, NY) and results were shown as mean \pm standard deviation (SD). In this study, $p < 0.05$ was considered as statistically significant in two-tailed tests.

3. Results and Discussion

3.1 *In vitro* characterization and biocompatibility

First, our ultrastructural analysis of the MagNP-OH used in this study allowed us to confirm that the diameter of the particles was 70 ± 18 nm, which is higher than MNPs frequently used by other authors in tissue engineering applications (30-40 nm) [15, 16, 37-41]. Interestingly, particles tended to form polycrystalline aggregates externally coated by a polymeric matrix surrounding each aggregate (Figure 1A). Magnetic characterization of the MagNP-OH revealed the typical soft ferromagnetic character of these MNPs, with negligible remnant magnetization, and a saturation magnetization of 161 ± 7 kA/m (Figure 1B). It is well known that the size of the MNPs is directly related to the magnetic response of the particles, and multidomain MNPs (> 50 nm) commonly show higher magnetic response as compared to small particles [38]. However, it has been previously demonstrated that biointegration of large MNPs in a hydrogel mesh tend to be incomplete due to gravitational settling and lower total surface area of these MNPs [14]. Although MNPs with a larger diameter will show stronger magnetic response [14], the present work was carried out with smaller nanoparticles in order to favour biointegration in the fibrin-agarose mesh. Further research is in need to determine the optimal size of the MNPs for use in the generation

of magnetic hydrogels, and the possibility of using particles of different sizes in the same hydrogel. In fact, the *in vivo* biological effects of MNPs have been demonstrated to be size-dependent [42].

Regarding *in vitro* cytocompatibility of human cells cultured in the presence of MagNP-OH, we carried out a multi-level approach analysis at three levels: cell morphology, cell function and integrity of the cell membrane. Results show that, in general, MNPs are highly cytocompatible. In the first place, co-culture of these MNPs with human cells was not able to modify the typical elongated spindle-like shape of viable human fibroblasts, suggesting that these cells remained highly viable, and MNPs were mostly found homogeneously distributed in the extracellular space of the cells (Fig. 1C). In fact, the morphology of these cells was comparable to positive control cells cultured without MNPs and very different from the small, rounded-shape appearance of negative control dead cells. To confirm these results at the functional level, we then analysed the functionality of the cellular mitochondrial dehydrogenase by WST-1 assay. Results showed high levels of metabolic activity in cells containing MagNP-OH (at the concentration of 1% and 0.5%) with values comparable ($p > 0.05$) to the positive control group. Positive controls and both experimental groups containing MagNP-OH showed significantly higher WST-1 values as compared to the negative control group ($p < 0.0001$) (Figure 1D), suggesting high metabolic activity [20, 28]. Finally, viability was analysed at the structural level by quantifying released DNA from cells cultivated in the presence of the MagNP-OH (Figure 1E), which is unfailingly associated to a cell membrane disruption [20, 28]. Results showed low cell mortality in positive controls and both experimental groups (1% and 0.5%), with no differences between positive controls and cells cultured with MagNP-OH ($p > 0.05$). However, mortality was significantly higher in negative controls ($p = 0.0020$). These results are in agreement with the high cytocompatibility previously observed in hydrogels containing MagNP-OH [17], especially when these particles were coated with a polymer such as polyethylene glycol (PEG) [14]. The polymeric coating of MNPs provides hydrophilic properties that may improve stabilization in colloidal suspension and increase biocompatibility [10, 43]. Altogether, these results support the high *in vitro* biocompatibility of the coated MagNP-OH used in this study.

Once the cytocompatibility of MagNP-OH was evaluated *in vitro*, we generated magnetic tissue-like biomaterials containing these particles. The rheological characterization of FAH-MNPs and FAH-MNPs-F revealed that incorporation of MagNP-OH considerably increased the strength of the tissue-like biomaterials as compared to control nonmagnetic FAH for the complex viscoelastic modulus

$$G^* = \left[(G')^2 + (G'')^2 \right]^{1/2} \text{ (Figure 1F), for both}$$

the biomaterials subjected to magnetic fields during the polymerization and materials devoid of these fields. In agreement with our previous studies [20, 28, 36], SEM images confirmed that the use of a magnetic field induced the alignment of the MNPs within the fibrin-agarose network (Figure 2). These findings are in agreement with previous reports showing that MNPs can considerably improve the biomechanical properties of FAH, thus increasing their putative usefulness in tissue engineering and regenerative medicine [13, 14, 17]. Previous studies suggest that the biomechanical improvement observed by the incorporation of MNPs within FAH can be explained by two reasons: on the one hand, the strong electrostatic interactions established between the biomaterial network and the MNPs, and on the other hand, the formation of MNPs clusters within the biomaterials network [17]. The electrostatic interactions increase the overall molecular interaction forces of the resulting biomaterial network, therefore explaining the biomechanical improvement. Furthermore, it was demonstrated that the MNPs clusters act as knots, sites from where the fibrin network is organized in more compact, thicker and aligned fibrin strands

which create a biomechanically and structurally more efficient network as compared to the classical nonmagnetic hydrogels [17].

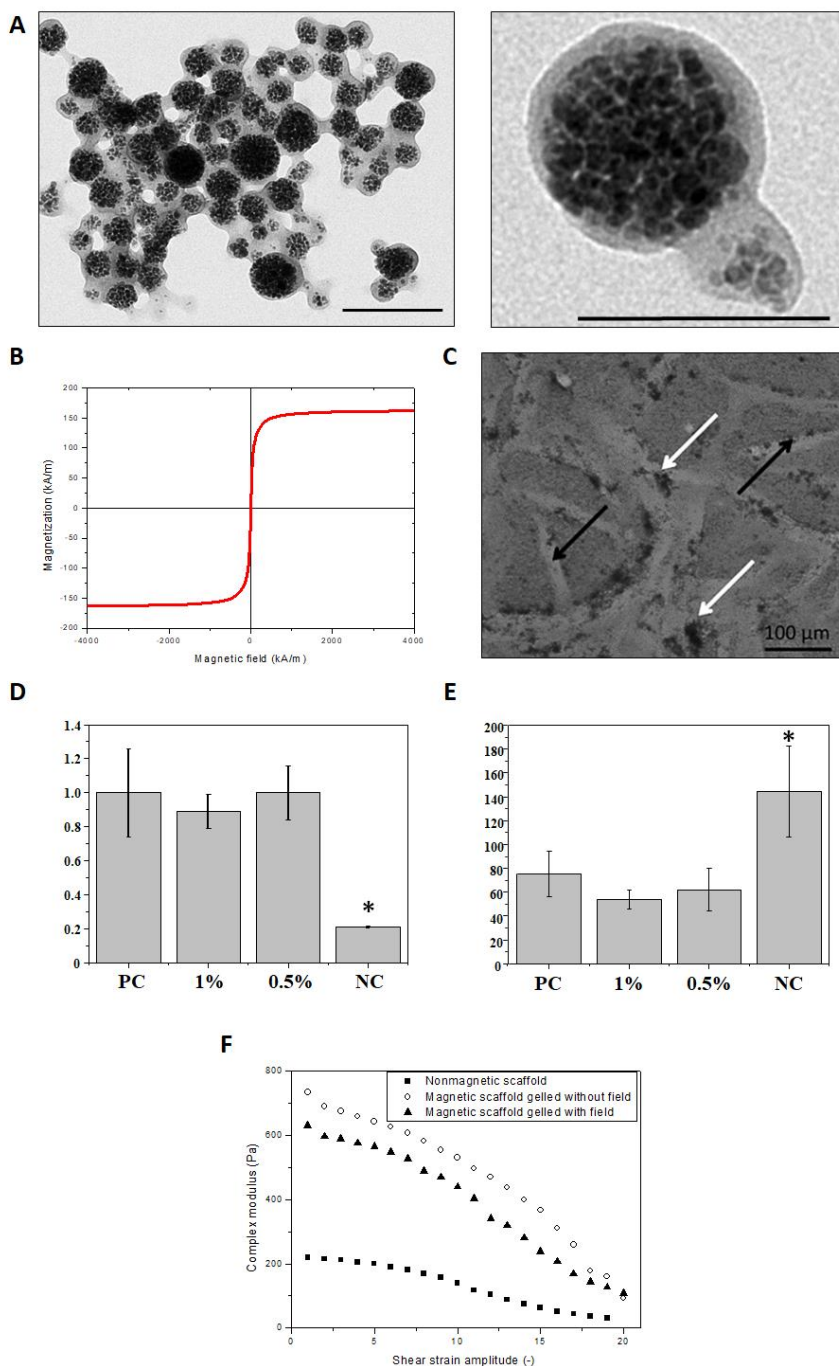


Figure 1. *In vitro* characterization of the MagNP-OH particles used in this study. A) Transmission electron microscopy ultrastructural analysis of MagNP-OH particles. Scale bar: 200 nm (left) and 100 nm (right). B) Magnetization curve of MagNP-OH particles. C) Phase contrast microscopy image of human fibroblasts cultured with MagNP-OH particles. Cells are labelled with black arrows and MagNP-OH particles are highlighted with white arrows. D) Results of the cellular metabolic activity as determined by WST-1 assay. E) Analysis of cell membrane integrity as determined by DNA quantification. In D and E, values correspond to averages and standard

deviations.* Results are statistically different from all the other study groups. PC: positive controls; NC: negative controls. F) Biomechanical properties are shown as the complex viscoelastic modulus of nonmagnetic FAH, FAH-MNPs and FAH-MNPs-F.

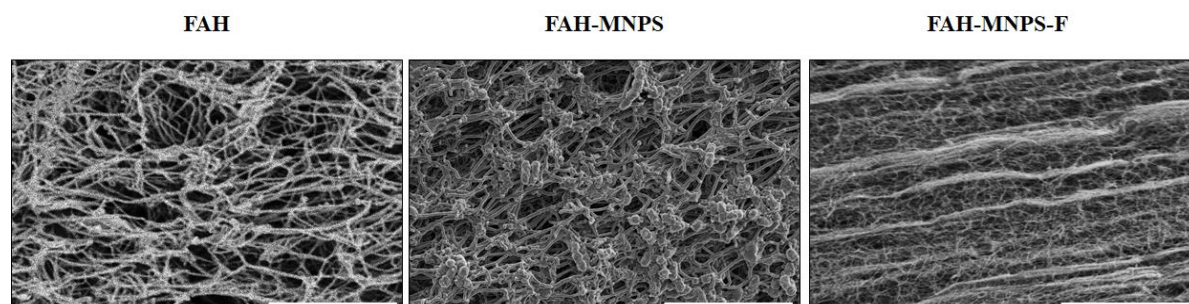


Figure 2. Representative images corresponding to the SEM analysis of materials used in this study. FAH: fibrin-agarose hydrogels; FAH-MNPs: FAH containing MagNP-OH; FAH-MNPs-F: FAH containing MagNP-OH subjected to a magnetic field during gelation. Scale bar 10 μ m

3.2 *In vivo* evaluation

Accurate monitoring and analysis of the fate of MNPs grafted *in vivo* in laboratory animals is essential for their future clinical translation and practical application [44]. Ideally, the biocompatibility of grafted MNPs should be assessed by using a combination of invasive and non-invasive methods allowing a precise evaluation of the fate of the MNPs and the potential metabolic pathways and organs involved in MNPs metabolism and biodegradation. Consequently, animals grafted with the different materials were subjected to an array of highly accurate evaluation methods that included MRI, magnetometry, haematological, biochemical and histological analyses to determine biocompatibility and the outcome of the grafted materials. In addition, analyses were performed at the local and the distal level as requested by most National Medicines Agencies for Advanced Therapies Medicinal Products [45]. In this sense, we first analysed the local graft site to determine *in situ* biosafety, temporal stability and migration to neighbour tissues. Then, we analysed four key distal organs to shed light on the possible distal effects of the grafted biomaterials, including distal organ migration. In general, all these analyses allowed us to demonstrate that the biomaterials used in the present work were safe and complied with the main biosafety requirements for future clinical use.

In situ time-course analysis of the implant site using MRI (Fig. 3) showed that non-magnetic FAH remained at the grafting site and was locally metabolized and reabsorbed in 12 weeks. In contrast, magnetic biomaterials containing MagNP-OH, as well as the injected MagNP-OH remained located in the implant site after 12 weeks of *in vivo* follow-up (Fig. 3). These results coincide with the magnetometric analyses showing that controls and animals grafted with FAH were negative, whereas all animals with grafted MagNP-OH showed a highly positive magnetic response at the grafting site after 12 weeks of follow-up. Furthermore, the MRI analysis of distal organs did not reveal any sign of damage, inflammation or organ failure in any of the experimental groups during the whole follow-up period (Supplementary Fig. S1).

MRI AT THE IMPLANTATION SITE

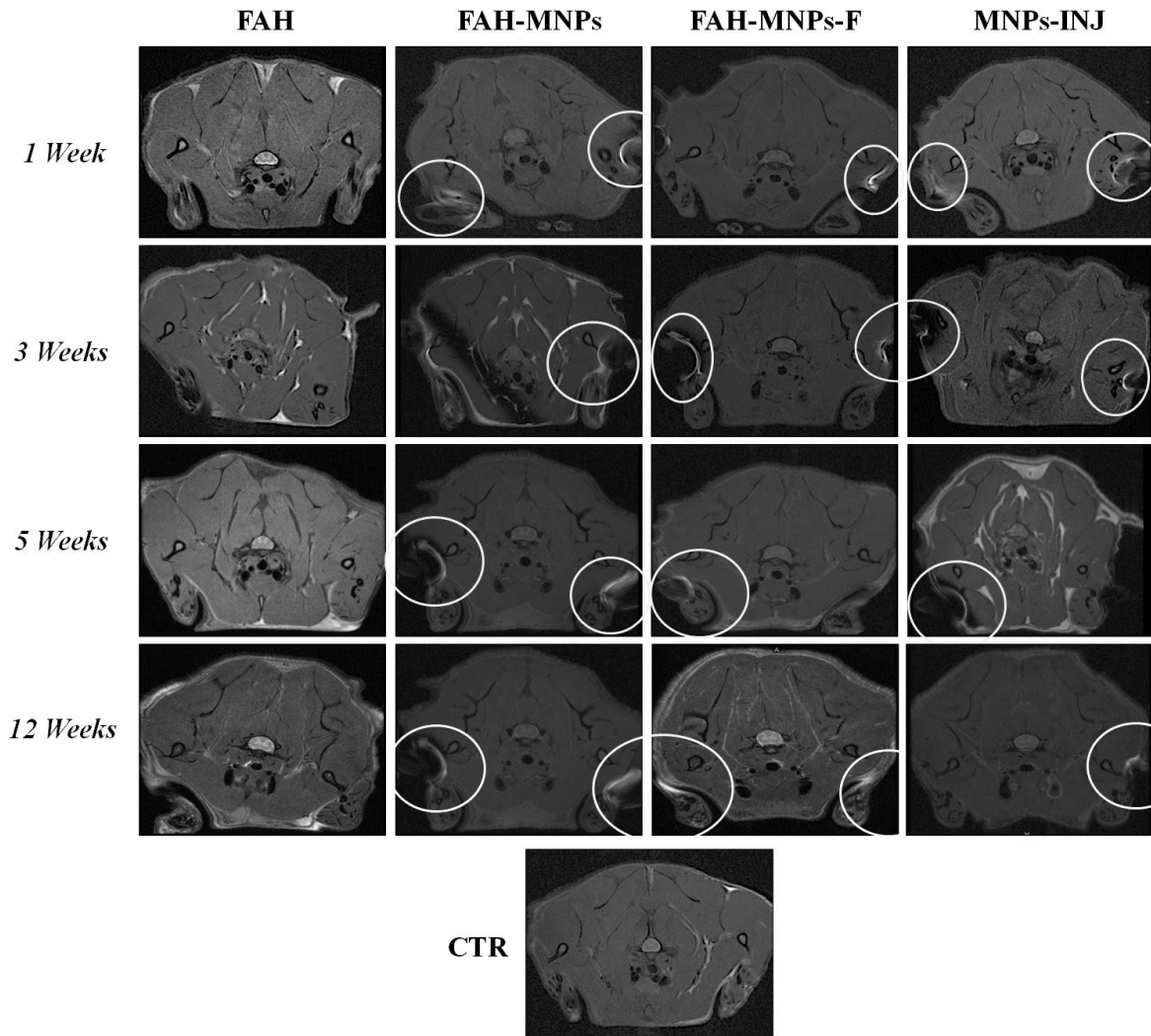


Figure 3. Magnetic Resonance Images (MRI) analysis of animals with the different materials grafted at each study time. Images were taken at the grafting site. White circles correspond to hyperintense areas corresponding to MagNP-OH accumulation at the implantation site. CTR: control animals; FAH: fibrin-agarose hydrogels; FAH-MNPs: FAH containing MagNP-OH; FAH-MNPs-F: FAH containing MagNP-OH subjected to a magnetic field during gelation; MNPs-INJ: MNPs injected subcutaneously.

Then, the implantation site was analysed histologically. In this regard, most animals showed an initial mild local inflammatory reaction restricted to the tissues surrounding the implanted materials, but no signs of necrosis, infection, rejection or malignant transformation were found in any of the groups (Fig. 4). This reaction was similar in all groups grafted with biomaterials (FAH, FAH-MNPs and FAH-MNPs-F), and tended to decrease over time. In the FAH group, we found that the number of inflammatory cells, especially macrophages, decreased with time and almost disappeared after 12 weeks. An interesting finding of our study was that the three groups in which MNPs were grafted tended to encapsulate the grafts, with the formation of a central Perls-positive nucleus surrounded by a connective tissue capsule. Although we found a single nucleus in the FAH-MNPs and FAH-MNPs-F groups, particles tended to form several independent nuclei in the MNPs-INJ group, at least during the

first 5 weeks (Fig. 4). These results confirm the absence of an increased inflammatory reaction driven by the MNPs implant and point out the usefulness of the FAH-MNPs model as a straightforward way of providing the host tissue with MNPs that could exert a positive clinical effect [46, 47]. As compared to injection, surgical implantation of a tissue-like magnetic material allowed a more efficient control of the grafting site and, according to our results, favoured the MNPs containment and enhanced encapsulation of the whole grafted mass in a single nucleus, thus preventing the connective tissue infiltration and grafts disaggregation or dispersion found in the MNPs-INJ group. In addition, the MNPs corresponding to the FAH-MNPs-F group showed a clear definite alignment and orientation of the MNPs during the first weeks, even though this orientation was lost after 5 weeks. Interestingly, the loss of this characteristic alignment pattern obtained by the use of a magnetic field coincided with the *in vivo* biodegradation process of the FAH [34]. In this regard, we recently demonstrated that FAH biomaterials are progressively remodelled and infiltrated by host immune cells, mainly macrophages, being completely degraded after 5 to 9 weeks of *in vivo* implantation [23, 34]. We may hypothesize that the progressive degradation and remodelling of the FAH network supporting the aligned particles resulted in a loss of structural cohesion of the aligned MNPs clusters with the consequent loss of its aligned structural pattern [23, 34]. The three-dimensional orientation of biomaterials is one of the goals of current tissue engineering, since most human tissues are characterized by a nonlinear and anisotropic mechanical behaviour [48] due to the non-random distribution of its components, and this distribution is essential for its proper *in vivo* function. The use of FAH-

MNPs-F could contribute to obtaining MNPs-based bioartificial tissues with defined alignment with added value for use in regenerative medicine [49], as shown in Fig. 2.

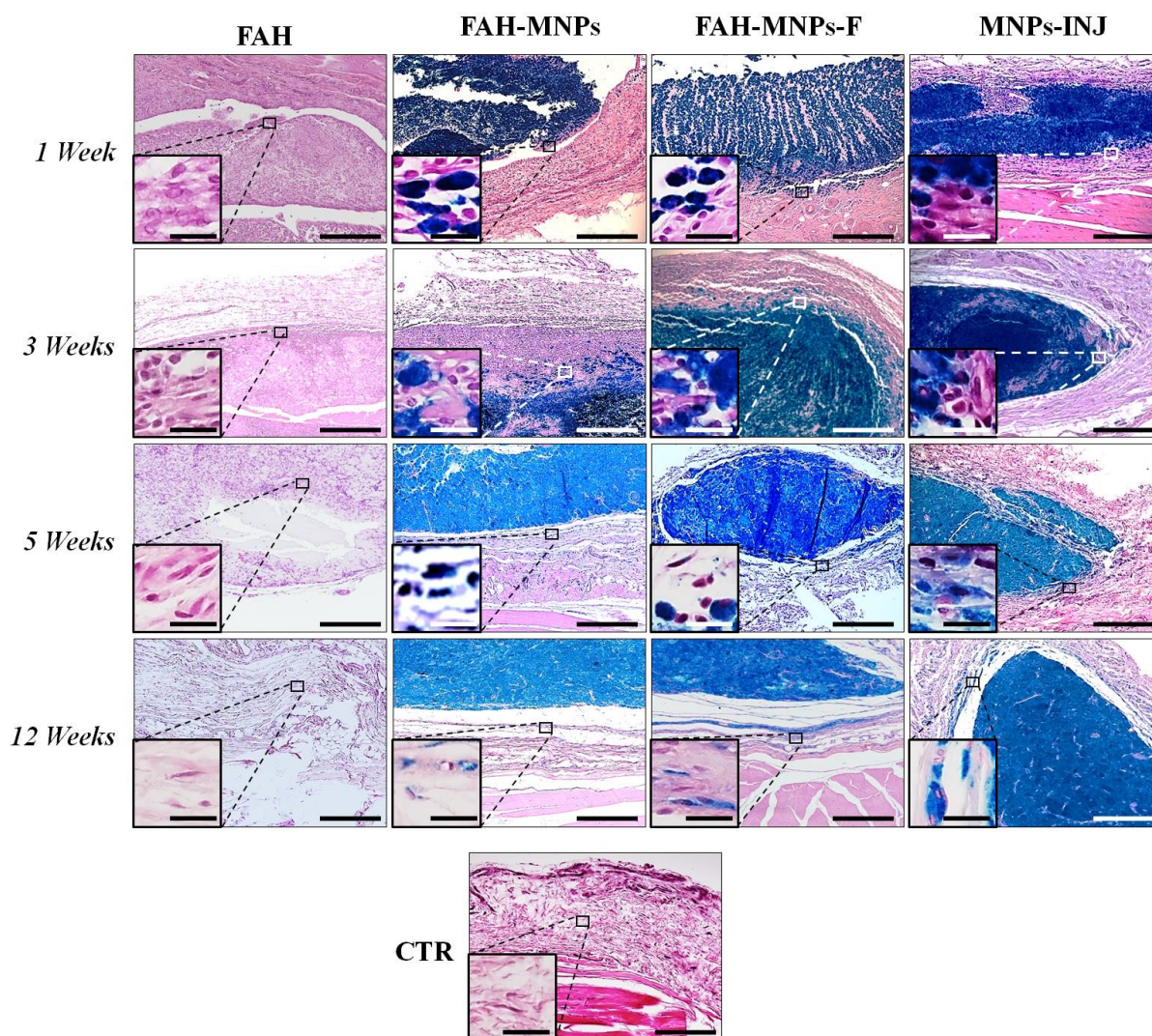


Figure 4. Perl's histochemical results of grafted biomaterials and injected MNPs at 1, 3, 5 and 12 weeks *in vivo*. CTR: control animals; FAH: fibrin-agarose hydrogels; FAH-MNPs: FAH containing MagNP-OH; FAH-MNPs-F: FAH containing MagNP-OH subjected to a magnetic field during gelation; MNPs-INJ: MNPs injected subcutaneously. The inserts images correspond to higher magnifications of the same images. Scale bars: 300 μ m (large images) and 20 μ m (inserts).

Furthermore, we carried out TEM analyses to determine the biocompatibility of each biomaterial at the ultrastructural level after 12 weeks of the surgical procedure. On the one hand, host tissues corresponding to the FAH group showed some macrophages with intracellular phagosomes containing rests of the biomaterial, along with extracellular matrix mainly consisting of collagen fibres that were comparable to control tissues (Fig. 5). On the other hand, animals grafted with MNPs showed very similar behaviour regardless of the specific group considered (FAH-MNPs, FAH-MNPs-F and MNPs-INJ). In all these groups, we found numerous host cells compatible with macrophages containing abundant intracellular MNPs that tended to keep their original

polycrystalline aggregate pattern inside the cells. Most of the particles gathered in cytoplasmic vesicles that could correspond to endosomes or secondary lysosomes, as well as large phagosomes. MagNP-OH were also found in the extracellular space. No signs of necrosis or cell alterations were detected in any of the study groups. These findings confirm the high biocompatibility of the different materials used in this study. In agreement with previous reports, our results suggest that iron oxide nanoparticles are mostly engulfed within the human cells and do not cause any detectable alterations in these cells [10, 50].

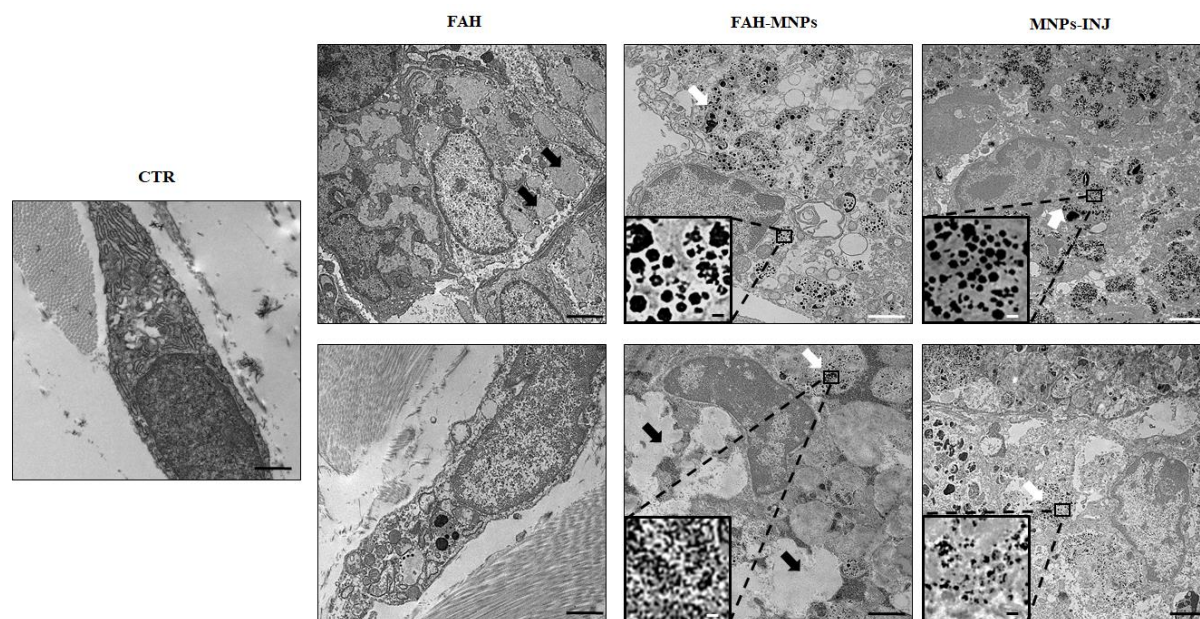


Figure 5. Representative images corresponding to the ultrastructural analysis of materials grafted *in vivo* for 12 weeks. CTR: control animals; FAH: fibrin-agarose hydrogels; FAH-MNPs: FAH containing MagNP-OH; MNPs-INJ: MNPs injected subcutaneously. Black arrow: phagosome containing agarose; white arrow: MNPs. The inserts images correspond to higher magnifications of the same images. Scale bars: 300 μm (large images) and 20 μm (inserts).

Once the local implant site was analysed, we evaluated the morphology, structure and function of several major distal organs of each animal to determine the possible distal effects of each biomaterial as part of the global biocompatibility and biosafety assessment required for future clinical use [45]. In this regard, the whole-body MRI scan analysis of each animal and the specific analysis of four key organs playing a role in metabolizing and processing a biomaterial grafted *in vivo* -liver, kidneys, lymph nodes and spleen- revealed a perfectly normal morphology devoid of detectable alterations (Supplementary Fig. 1). No MNPs were detected by MRI in any of these organs. Similarly, analysis of the different organs using magnetometry, revealed a negative signal in all animals after 12 weeks of *in vivo* follow-up. These results suggest that MagNP-OH stayed at the grafting site and did not tend to migrate, supporting the stability of this type of MNPs.

At the histological level, the structural analysis of distal organs confirmed the absence of alterations during the whole study. Indeed, no signs of inflammation, fibrosis, necrosis or other detectable tissue alterations were observed in histological sections of liver, kidneys, lymph nodes and spleen stained with H&E in any of the groups (Supplementary Fig. S2). Similarly, PAS staining analysis (Supplementary Fig. S3) confirmed that the content of

glycogen was normal in hepatocytes of all groups of animals, and the glomerular and non-glomerular basement membranes were also free from detectable alterations. These results are in agreement with previous studies demonstrating that this type of MNPs coated with different polymers can be safely used without significant histological alterations of vital organs [14, 51], whereas other types of particles were associated to histological lesions in liver and kidney [52].

To identify any possible particle migration to distal organs, we also analysed these organs using the Perls histochemical technique, which is specific for detection of iron in cells and tissues. Results showed very few or no particles in the liver and kidney at 1 and 12 weeks, but a positive reaction was found in spleen and lymph nodes at both analysed times (Fig. 6). These findings are in agreement with previous reports demonstrating that nanoparticles of different nature tend to be massively captured by cells of the mononuclear phagocyte system [49]. Hence, we found that lymph nodes were Perls-negative in CTR and FAH group, whereas animals with grafted MNPs (FAH-MNPs, FAH-MNPs-F and MNPs-INJ) showed small Perls-positive areas after 1 week, and moderate to intense Perls-positive areas after 12 weeks, especially in the case of the injected MNPs. Then, we analysed both components of the rat spleen (the red and the white pulp), and we found that the staining area and intensity were higher in this organ than in the rest of organs. As expected, the red pulp of the spleen was very positive to the Perls method in all groups, including controls, but this reaction became significantly more intense after 12 weeks in FAH-MNPs, FAH-MNPs-F and MNPs-INJ groups ($p < 0.05$). These findings are consistent with the primary function of the red pulp, which is related to filtering peripheral blood from antigens, foreign bodies and all kinds of substances that may arrive in the blood, blood iron turnover, as well as serving as a huge reservoir of monocytes [18]. The white pulp, however, was mostly negative for this staining technique, although the marginal zone (in which antigen-presenting cells, such as dendritic cells and macrophages exists) was positive at 12 weeks in FAH-MNPs, FAH-MNPs-F and MNPs-INJ groups. Quantification of the Perls-positive areas in the red pulp (Fig. 7) demonstrated no significant differences among samples at 1 week ($p > 0.05$), but a significant increase was found at 12 weeks in the FAH-MNPs and MNPs-INJ groups ($p < 0.05$). In fact, the three groups in which MNPs were grafted in animals, showed significant differences vs. control at week 12 ($p < 0.05$). These results were corroborated at the ultrastructural level by TEM analysis confirming the presence of macrophages containing electron-dense iron-rich granular material identified as iron by EELS in all experimental groups (Fig. 7). In contrast with the macrophages observed within grafted biomaterials, in spleen, these cells contained iron-rich granular intracytoplasmic vesicles, but polycrystalline aggregates were not detected.

The presence of abundant cells containing iron in the spleen of all animal groups could be explained by the important role that the spleen plays in mechanical filtration of red blood cells and haemoglobin iron recycling and turnover [18]. The increase observed in animals in which MagNP-OH were grafted, strongly suggests that MNPs could progressively reach to the spleen through blood circulation, as other authors demonstrated by intraperitoneal injection of RITC-labeled MNPs [10, 50]. The fact that our magnetometry and MRI analyses were negative could probably be explained by the low concentration of MagNP-OH that reached the spleen, which was probably below than 30 μg , which is the minimum concentration required for detection by magnetometry and MRI. Another possibility is that MagNP-OH were progressively transformed into non-magnetic iron forms by host cells as previously suggested [47]. Interestingly, previous works showed that superparamagnetic iron-oxide NPs show identical distribution pattern when administered *in vivo* [51].

In consequence, our histological results, in line with results published by other authors, highlight the relevance of the administration route and NPs size in the subsequent organic biodistribution [10], and confirm that MagNP-OH

tend to remain stable at the implant site, with some particles biodistributed to lymphoid organs, without altering their histological structure and function.

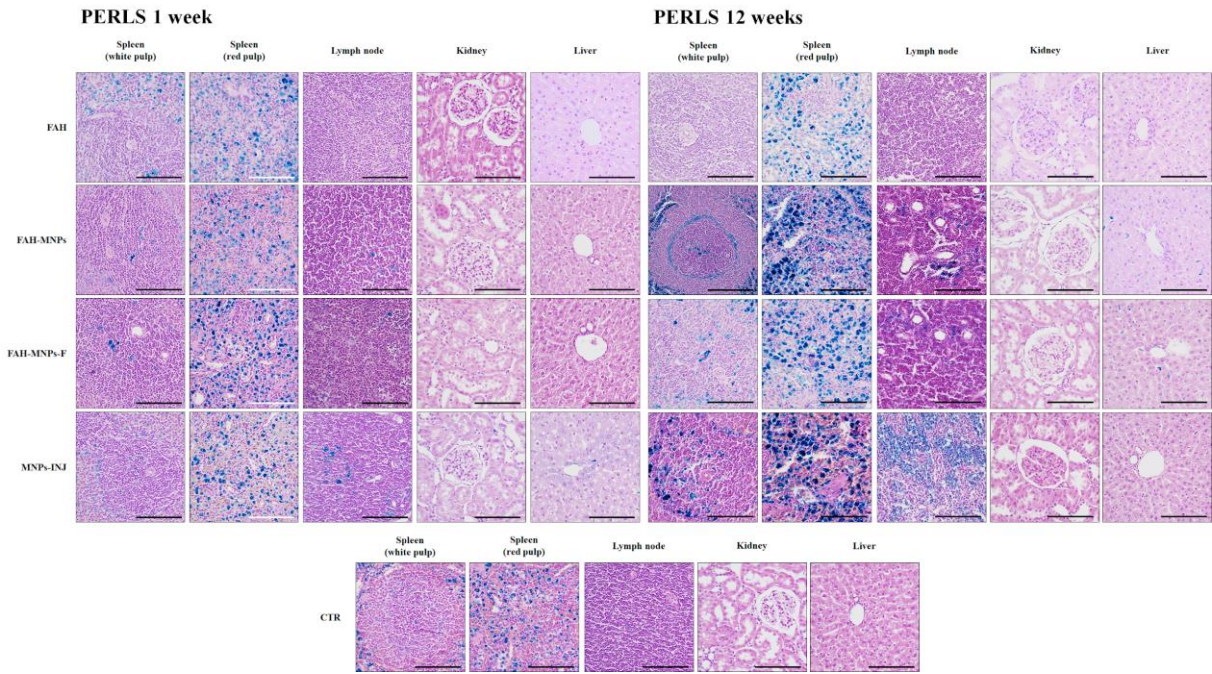


Figure 6. Perl's histochemical results of distal organs at 1 and 12 weeks. FAH: fibrin-agarose hydrogels; FAH-MNPs: FAH containing MagNP-OH; FAH-MNPs-F: FAH containing MagNP-OH subjected to magnetic field during gelation; MNPs-INJ: MNPs injected subcutaneously; CTR: control animals. Scale bar 100 μ m.

PERLS-POSITIVE AREAS IN SPLEEN RED PULP	CTR	FAH	FAH-MNPs	FAH-MNPs-F	MNPs-INJ
1 week	3.28 ± 0.55	3.54 ± 0.75 (p = 0.9990)	5.77 ± 0.61 (p = 0.4977)	9.64 ± 1.38 (p = 0.0818)	8.61 ± 0.72 (p = 0.1338)
12 weeks	7.77 ± 0.89	5.43 ± 0.15 (p = 0.5679)	22.84 ± 1.83 (p = 0.0056)*	18.62 ± 1.81 (p = 0.0370)*	28.25 ± 2.45 (p = 0.0004)*
1 week vs. 12 weeks	(p = 0.2134)	(p = 0.9990)	(p = 0.0010)*	(p = 0.1070)	(p = 0.0009)*

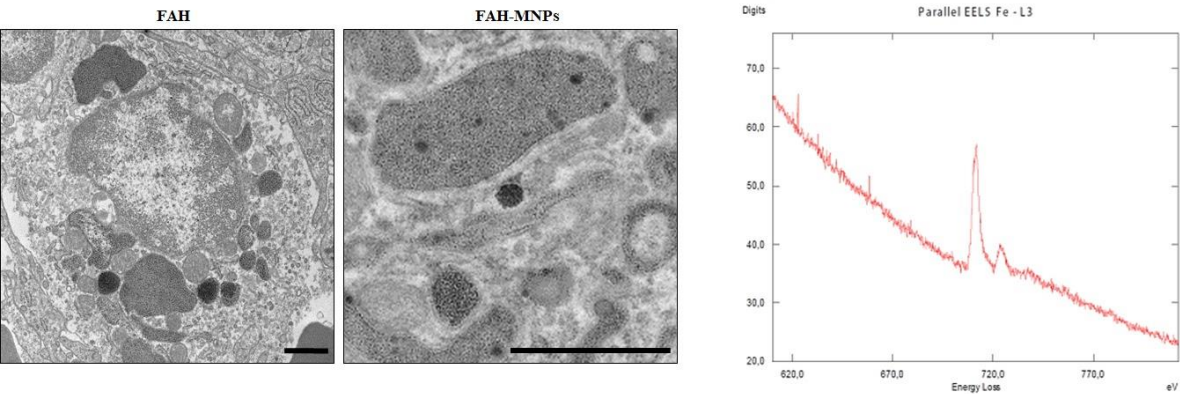


Figure 7. Quantitative results of Perls positive histochemical reaction and EELS in the red pulp of the spleen in each group and control. The table on top shows the results of the quantification of the percentage of the area corresponding to Perls-positive signal. The figures below show illustrative ultrastructural images of macrophages containing iron in intracellular phagosomes corresponding to two groups of animals (FAH and FAH-MNPs), along with an EELS spectrum with a peak corresponding to intracellular iron. CTR: control animals; FAH: fibrin-agarose hydrogels; FAH-MNPs: FAH containing MagNP-OH; FAH-MNPs-F: FAH containing MagNP-OH subjected to a magnetic field during gelation; MNPs-INJ: MNPs injected subcutaneously. Values in the table are shown as mean ± standard deviation for each group of animals and each follow-up time, and the statistical p values corresponding to the comparison of these values with CTR are shown in brackets. In the last row, the statistical p values corresponding to the comparison of values at 1 week vs. values at 12 weeks are shown for each study group. Significant differences ($p < 0.05$) are highlighted with asterisks (*). Scale bar for FAH = 1 μm and scale bar for FAH-MNPs = 2 μm .

		HAEMOGRAM							Weeks	
		General count					WBC/White cells			
		WBC (10 ³)	RBC (10 ⁶)	HGB	HCT	PLT (10 ⁵)	LYM	MXD		NEUT
		μL ⁻¹	μL ⁻¹	g/dL	%	μL ⁻¹	%	%		%
FAH	3.04 ± 1.51*	7.14 ± 0.22*	13.5 ± 0.52	39.54 ± 1.1	5.16 ± 1.99	45.68 ± 23.56	32.56 ± 22.96	21.76 ± 4.64	1	
	4.56 ± 3.31	7.61 ± 0.06	14.14 ± 0.51	42.28 ± 0.66	4.60 ± 2.59	64.38 ± 14.8	12.96 ± 0.86	22.66 ± 14.22	3	
	2.75 ± 0.26*	8.04 ± 0.4	14.15 ± 0.27	43.78 ± 1.3	6.57 ± 0.23	77.63 ± 4.06	9.25 ± 3.02	13.13 ± 5.75	5	
	9.74 ± 3.89	8.15 ± 0.38	14.32 ± 0.2	44.06 ± 1.93	5.11 ± 3.63	68.5 ± 16.18	9.32 ± 3.65	22.18 ± 13.58	12	
FAH-MNPs	2.4 ± 1.27	7.47 ± 0.64	13.22 ± 1.48	40.02 ± 4.35	5.63 ± 2.96	42.08 ± 26.77	33.02 ± 25.75	24.84 ± 12.87	1	
	5.18 ± 3.11	7.51 ± 0.3	14.16 ± 0.76	42.26 ± 2.17	3.82 ± 2.16	62.02 ± 15.52	13.34 ± 2.57	24.64 ± 16.25	3	
	2.48 ± 1.09	8.11 ± 1.48*	14.18 ± 9.93	44.27 ± 1.72	6.24 ± 2.57	72.7 ± 16.81	5.92 ± 1.78	21.08 ± 9.9	5	
	2.94 ± 3.52	7.83 ± 0.68	14.16 ± 0.76	42.48 ± 4.15	8.74 ± 0.84	80.32 ± 3.35 *	15.28 ± 4.59	2.56 ± 5.96	12	

FAH-MNPs-F	3.63 ± 2.1	7.76 ± 0.38	13.83 ± 0.25	42.43 ± 1.85	5.61 ± 1.21	66.25 ± 8.58	13.83 ± 5.93	19.93 ± 6.41	1
	2.46 ± 0.46	7.62 ± 0.44	13.58 ± 0.39	41.18 ± 1.69	6.31 ± 0.72	76.02 ± 3.35	11.04 ± 1.35	12.94 ± 2.11	3
	5.36 ± 4.05	7.77 ± 4.09*	13.91 ± 0.6	42.73 ± 1.81	3.62 ± 2.48	68 ± 12.91	16.02 ± 7.07	15.98 ± 6.97	5
	5.72 ± 1.73	8.46 ± 0.62*	14.52 ± 0.6	45.66 ± 3.1	3.78 ± 4.1	69 ± 13.41	12.64 ± 2.97	18.36 ± 11.6	12
MNPs-INJ	2.48 ± 0.43	7.82 ± 0.24	13.78 ± 0.42	42.8 ± 1.86	4.88 ± 2.75	72.08 ± 6.03	12.53 ± 1.24	15.4 ± 6.02	1
	1.92 ± 0.64	7.54 ± 0.26	13.5 ± 0.24	41.22 ± 1.51	6.26 ± 0.73	73.2 ± 7.71	14.92 ± 5.72	11.88 ± 2.58	3
	1.78 ± 0.29	8.03 ± 0.23 *	14.08 ± 0.83	43.94 ± 2	5.94 ± 2.82	74.5 ± 3.71	10.82 ± 4.98	14.68 ± 6.67	5
	7.1 ± 3.74	7.57 ± 0.89	13.75 ± 1.61	41.45 ± 5.4	4.33 ± 4.58	65.83 ± 4.67	10.03 ± 3.42	24.15 ± 6.5	12
CTR	5.93 ± 3.46	7.72 ± 0.11	13.9 ± 0.5	42.25 ± 1.07	2.58 ± 2.71	63.03 ± 15.39	14.33 ± 6.75	22.65 ± 13.16	

Table 1. Haematological profile. Summary of the mean and SD of parameters evaluated at 1, 3, 5 and 12 weeks. White blood cells (WBC), erythrocytes count (RBC), concentration of haemoglobin (HGB), haematocrit count (HCT), platelets (PLT), lymphocytes (LYM), monocytes-basophils-eosinophils (MXD), neutrophils (NEUT). Significant differences ($p < 0.05$) between experimental and control groups are highlighted with asterisks (*).

After that the morphology and structure of local and distal tissues and organs were determined, we analysed the effect of the different biomaterials on each animal group at the functional level. In this regard, haematological studies revealed that all parameters evaluated here were within the physiological range of normal values described in the literature for the Wistar rat (Table 1) [52]. However, some specific parameters showed significant differences with the control animals used in this study. In the case of the red blood cells (RBC), we observed a significant decrease of RBC counts in the FAH group at 1 week as compared to controls ($p = 0.009$), which could be a consequence of the recent surgical procedure. In contrast, a significant increase of the number of RBC was observed after 5 weeks in FAH-MNPs ($p = 0.016$), FAH-MNPs-F ($p = 0.016$) and MNPs-INJ ($p = 0.028$), and also after 12 weeks for FAH-MNPs-F ($p = 0.028$) as compared to controls. Interestingly, the increase of RBC values was not accompanied by significant variations of the concentration of haemoglobin (HGB) or haematocrit (HCT). The leukocyte count (WBC) showed a transient reduction in the FAH group at 5 weeks as compared to controls ($p = 0.009$), although the leukocyte formula was normal for all the study groups except for an increase of lymphocytes (LYM) at 12 weeks in FAH-MNPs group ($p = 0.010$). Finally, the evaluation of platelets (PLT) showed an increase in all experimental groups over time as compared to control animals. All these variations, which fell into the normal parameters of healthy Wistar rats [52], could be related to the host adaptive physiological response to the surgical procedure, healing process, active hydrogel biodegradation and MagNP-OH phagocytosis being these results in line with the histological findings. A similar result was found for the biochemical parameters analysed in plasma of each animal, which were normal in most cases (Table 2). First, the levels of circulating iron were similar to control animals at all study times ($p > 0.05$). The lack of increase of circulating free iron supports the idea that MNPs remained stable and were not able to release a significant amount of iron to the circulation. Similarly, most hepatic function-related parameters fell within the physiological range of this species, except for an initial transient decrease of ALT in MNPs-INJ ($p = 0.028$) that normalized thereafter. Finally, the two biochemical markers of renal function (urea and creatinine) were normal in all study groups. Additionally, the renal function-related parameters urea and creatinine (CREJ2) showed a transitory increase over the time in all experimental groups as compared to controls, which tended to normalize with time.

Altogether, these haematological and biochemical results confirmed that the use of MagNP-OH is safe and *in vivo* implantation of these MNPs is not associated to a vital organ failure. Although some slight variations were found in specific groups of animals, values were in agreement with the physiological ranges described in the literature

[52], and showed a clear normalization over time. In addition, the normalization of blood and biochemical parameters is in line with the quantitative results observed in Wistar rats in which the sciatic nerve was repaired with acellular nerve grafts [35]. These findings confirm again that both administration routes for the MagNP-OH (injected or encapsulated) were safe for the host animal. In contrast, a previous study showed that the high-dose oral administration of other types of nanoparticles based on silver was related to hepatic and renal affection at the biochemical level, what clearly differed from our findings [52]. Finally, the haematological and biochemical profiles were in concordance with the histological and MRI results showing normal structure and morphology of distal organs. All this suggests that the *in vivo* injection and the subcutaneous implantation of the magnetic materials generated in this work was fully biocompatible and fulfilled the strict biosafety criteria required for future clinical use.

		BIOCHEMICAL			
		Liver	Kidney		Other parameters
		ALT	CREJ2	UREA	Fe
		U/L	mg/dl	mg/dl	µg/dl
FAH	46.28 ± 10.26	0.75 ± 0.08	42.32 ± 6.71	162.27 ± 0.29	1
	40.44 ± 7.38	0.65 ± 0.14	43.28 ± 7.34	170.25 ± 0.33	3
	41.35 ± 17.39	0.6 ± 0.24	38.08 ± 13.76	164.21 ± 0.61	5
	53.54 ± 16.03	0.6 ± 0.08	36.94 ± 2.65	181.19 ± 0.22	12
FAH-MNPs	141 ± 144.53	0.7 ± 0.15	46.66 ± 8.73	147.31 ± 0.31	1
	79.2 ± 65.15	0.72 ± 0.08	43.84 ± 5.97	187.51 ± 0.32	3
	42.08 ± 10.65	0.66 ± 0.15	38.22 ± 2.67	171.19 ± 0.40	5
	74.68 ± 60.94	0.54 ± 0.11	35.08 ± 4.48	249.36 ± 1.91	12
FAH-MNPs-F	45.75 ± 6.72	0.84 ± 0.18	37.5 ± 8.76	157.85 ± 0.42	1
	46.82 ± 11.49	0.69 ± 0.1	41.5 ± 4.6	160.15 ± 0.15	3
	46.61 ± 26.92	0.53 ± 0.05	39.59 ± 4.93	172.2 ± 0.27	5
	45.28 ± 9.17	0.66 ± 0.05	38.72 ± 5.84	148.91 ± 0.10	12
MNPs-INJ	30.2 ± 7.83*	0.65 ± 0.11	39.3 ± 7.57	155.15 ± 0.25	1
	35.94 ± 6.19	0.53 ± 0.08	38.98 ± 4.74	183.92 ± 0.22	3
	62.86 ± 30.07	0.71 ± 0.11	38.56 ± 4.89	168.49 ± 0.26	5
	44.62 ± 10.09	0.74 ± 0.11	39.58 ± 5.2	164.91 ± 0.29	12
CTR	39.55 ± 5.55	0.46 ± 0.14	34 ± 2.81	184.36 ± 0.23	

Table 2. Biochemical profile. Summary of the mean and SD of parameters evaluated at 1, 3, 5 and 12 weeks. Alanine aminotransferase (ALT), urea (UREA), creatinine (CREJ2) and iron (Fe). Significant differences ($p < 0.05$) between experimental and control groups are highlighted with asterisks (*).

In summary, although the particles remained at the grafting site after 12 weeks, these results suggest that MagNP-OH fulfil the biosafety and biocompatibility requirements for future clinical use. Incorporation of these MNPs in fibrin-agarose biomaterials allows the generation of novel biomaterials with improved biomechanical properties with guarantees of biosafety and biocompatibility demonstrated at the morphological, structural and functional levels. As an alternative route of delivery, tissue-like biomaterials allow efficient control of the MNPs biodistribution *in vivo*. Biodistribution analysis demonstrated that our strategy supports the local use of the MagNP-OH, which were mostly confined to the implantation area. However, long-term studies are still needed to determine the time required for the complete biodegradation and/or metabolization of the implanted MagNP-OH. In addition, tissue-like biomaterials based on fibrin-agarose combined with MagNP-OH allows easy handling and straightforward surgical implant of these nanoparticles, and facilitates local *in vivo* encapsulation of MagNP-OH as compared to injected MagNP-OH. In addition, the methodology described in the present manuscript also

allowed the generation of novel biomaterials with a definite structural alignment using magnetic fields during the gelation of the biomaterial. This could be advantageous for reproduction and treatment of human tissues requiring a specific 3D structural organization such as the human cornea [53], tendon [54] and cartilage [55] and also other tissues with an anisotropic behaviour such as the human skin, nerve and oral mucosa and palate [56]. However, future clinical trials should demonstrate the usefulness of these tissue-like products.

4. Conflicts of interest

The authors declare that they have no known competing financial interests or personal relationships that could have appeared to influence the work reported in this paper.

5. Author contributions

MTLL performed magnetic particles characterization. IAR, MA developed *in vitro* analyses of biocompatibility. ABBE, MTLL, performed the mechanical properties. FC, IAR, ABBE, VC performed the surgery of animals. FC, IAR, VC performed and analysed the magnetic resonance imaging. IAR, ABBE, VC developed and analysed the data of haematological and biochemical studies. FC, IAR, ABBE, VC, developed histological and histochemical studies. IAR and VC analysed data of histology. RC, IAR, VC performed the ultrastructural study. MTLL, ABBE, PK, performed magnetometry. FC, MA, statistical analyses. IAR, FC, VC, MA performed the experimental design and wrote this work.

6. Acknowledgements

This study was supported by the following grants:

- Grants FIS-PI17/0391 and FIS-PI17/0393 from Instituto de Salud Carlos III - ISCIII (Plan Nacional de Investigación Científica, Desarrollo e Innovación Tecnológica I+D+i from the Spanish Ministerio de Ciencia e Innovación), co-financed by ERDF-FEDER, European Union.
- Award number AC17/00013 (NanoGSkin) by ISCIII thorough AES 2017 and within the EuroNanoMed framework.
- Grant MINECO FIS2017-85954-R from Agencia Estatal de Investigación (Spanish Ministerio de Asuntos Económicos y Transformación Digital), co-funded by Fondo Europeo de Desarrollo Regional, FEDER, European Union).
- Grants CS PI-0257-2017 and CSyF PE-0395-2019 from Consejería de Salud y Familias, Junta de Andalucía, Spain.
- Grant nº Res SECYT 411/18 from SECYT (Secretary of Science and Technology of National University of Córdoba, Argentina)
- Project Future Investments UCA JEDI, No. ANR-15-IDEX-01, project “RheoGel” by the French “Agence Nationale de la Recherche”.

Authors are grateful to Dr. Ariane Ruyffelaert for her proofreading service and for the technical assistance of Amalia de la Rosa Romero and Concepción López Rodríguez (Experimental Unit of the University Hospital Virgen de las Nieves, Granada, Spain).

References

- [1] A. Cervadoro, C. Giverso, R. Pande, S. Sarangi, L. Preziosi, J. Wosik, A. Brazdeikis, P. Decuzzi, *PLoS One*, 8 (2013) e57332.
- [2] K. Andreas, R. Georgieva, M. Ladwig, S. Mueller, M. Notter, M. Sittlinger, J. Ringe, *Biomaterials*, 33 (2012) 4515-4525.
- [3] X.W. Chen, Q.X. Mao, J.W. Liu, J.H. Wang, *Talanta*, 100 (2012) 107-112.
- [4] J. Qin, K. Li, C. Peng, X. Li, J. Lin, K. Ye, X. Yang, Q. Xie, Z. Shen, Y. Jin, M. Jiang, G. Zhang, X. Lu, *Biomaterials*, 34 (2013) 4914-4925.
- [5] S. Jiang, A.A. Eltoukhy, K.T. Love, R. Langer, D.G. Anderson, *Nano Lett*, 13 (2013) 1059-1064.
- [6] G.Y. Lee, W.P. Qian, L. Wang, Y.A. Wang, C.A. Staley, M. Satpathy, S. Nie, H. Mao, L. Yang, *ACS Nano*, 7 (2013) 2078-2089.
- [7] M.J. Alonso, S. Cohen, T.G. Park, R.K. Gupta, G.R. Siber, R. Langer, *Pharm Res*, 10 (1993) 945-953.
- [8] S. Behrens, *Nanoscale*, 3 (2011) 877-892.
- [9] K. Niemirowicz, K.H. Markiewicz, A.Z. Wilczewska, H. Car, *Adv Med Sci*, 57 (2012) 196-207.
- [10] L.H. Reddy, J.L. Arias, J. Nicolas, P. Couvreur, *Chem Rev*, 112 (2012) 5818-5878.
- [11] C. Chouly, D. Pouliquen, I. Lucet, J.J. Jeune, P. Jallet, *J Microencapsul*, 13 (1996) 245-255.
- [12] R. De Santis, A. Russo, A. Gloria, U. D'Amora, T. Russo, S. Panseri, M. Sandri, A. Tampieri, M. Marcacci, V.A. Dediu, C.J. Wilde, L. Ambrosio, *J Biomed Nanotechnol*, 11 (2015) 1236-1246.
- [13] M.T. Lopez-Lopez, G. Scionti, A.C. Oliveira, J.D. Duran, A. Campos, M. Alaminos, I.A. Rodriguez, *PLoS One*, 10 (2015) e0133878.
- [14] L. Rodriguez-Arco, I.A. Rodriguez, V. Carriel, A.B. Bonhome-Espinosa, F. Campos, P. Kuzhir, J.D. Duran, M.T. Lopez-Lopez, *Nanoscale*, 8 (2016) 8138-8150.
- [15] X.B. Zeng, H. Hu, L.Q. Xie, F. Lan, W. Jiang, Y. Wu, Z.W. Gu, *Int J Nanomedicine*, 7 (2012) 3365-3378.
- [16] N. Bock, A. Riminucci, C. Dionigi, A. Russo, A. Tampieri, E. Landi, V.A. Goranov, M. Marcacci, V. Dediu, *Acta Biomater*, 6 (2010) 786-796.
- [17] A.B. Bonhome-Espinosa, F. Campos, I.A. Rodriguez, V. Carriel, J.A. Marins, A. Zubarev, J.D.G. Duran, M.T. Lopez-Lopez, *Soft Matter*, 13 (2017) 2928-2941.
- [18] J.S. Kim, T.J. Yoon, K.N. Yu, B.G. Kim, S.J. Park, H.W. Kim, K.H. Lee, S.B. Park, J.K. Lee, M.H. Cho, *Toxicol Sci*, 89 (2006) 338-347.
- [19] M. Alaminos, M. Del Carmen Sanchez-Quevedo, J.I. Munoz-Avila, D. Serrano, S. Medialdea, I. Carreras, A. Campos, *Invest Ophthalmol Vis Sci*, 47 (2006) 3311-3317.
- [20] F. Campos, A.B. Bonhome-Espinosa, G. Vizcaino, I.A. Rodriguez, D. Duran-Herrera, M.T. Lopez-Lopez, I. Sanchez-Montesinos, M. Alaminos, M.C. Sanchez-Quevedo, V. Carriel, *Biomed Mater*, 13 (2018) 025021.
- [21] V. Carriel, I. Garzon, J.M. Jimenez, A.C. Oliveira, S. Arias-Santiago, A. Campos, M.C. Sanchez-Quevedo, M. Alaminos, *Cells Tissues Organs*, 196 (2012) 1-12.
- [22] V. Carriel, G. Scionti, F. Campos, O. Roda, B. Castro, M. Cornelissen, I. Garzon, M. Alaminos, *J Tissue Eng Regen Med*, 11 (2017) 1412-1426.
- [23] V. Carriel, G. Vizcaino-Lopez, J. Chato-Astrain, D. Durand-Herrera, M. Alaminos, A. Campos, I. Sanchez-Montesinos, F. Campos, *Exp Eye Res*, 186 (2019) 107717.

625 [24] J. Chato-Astrain, F. Campos, O. Roda, E. Miralles, D. Durand-Herrera, J.A. Saez-
626 Moreno, S. Garcia-Garcia, M. Alaminos, A. Campos, V. Carriel, *Front Cell Neurosci*, 12
627 (2018) 501.

628 [25] I.A. Rodriguez, M.T. Lopez-Lopez, A.C. Oliveira, M.C. Sanchez-Quevedo, A. Campos,
629 M. Alaminos, J.D. Duran, *J Tissue Eng Regen Med*, 6 (2012) 636-644.

630 [26] M.C. Sanchez-Quevedo, M. Alaminos, L.M. Capitan, G. Moreu, I. Garzon, P.V. Crespo,
631 A. Campos, *Histol Histopathol*, 22 (2007) 631-640.

632 [27] M. Lopez-Lopez, I. Rodriguez, L. Rodriguez-Arco, V. Carriel, A. Bonhome-Espinosa, F.
633 Campos, A. Zubarev, J. Duran, *Journal of Magnetism and Magnetic Materials*, 431 (2017)
634 110-114.

635 [28] F. Campos, A.B. Bonhome-Espinosa, L. Garcia-Martinez, J.D. Duran, M.T. Lopez-
636 Lopez, M. Alaminos, M.C. Sanchez-Quevedo, V. Carriel, *Biomed Mater*, 11 (2016) 055004.

637 [29] M.A. Rodriguez, M.T. Lopez-Lopez, J.D. Duran, M. Alaminos, A. Campos, I.A.
638 Rodriguez, *Cryobiology*, 67 (2013) 355-362.

639 [30] V. Carriel, I. Garzon, M. Alaminos, M. Cornelissen, *Neural Regen Res*, 9 (2014) 1657-
640 1660.

641 [31] Y. Li, H. Meng, Y. Liu, B.P. Lee, *ScientificWorldJournal*, 2015 (2015) 685690.

642 [32] S. Vieira, A. Morais, J. Silva-Correia, J. Oliveira, R.L. Reis, *Natural-Based Hydrogels:*
643 *From Processing to Applications*, 2017.

644 [33] L. Gasperini, J.F. Mano, R.L. Reis, *J R Soc Interface*, 11 (2014) 20140817.

645 [34] F. Campos, A.B. Bonhome-Espinosa, J. Chato-Astrain, D. Sanchez-Porras, O.D. Garcia-
646 Garcia, R. Carmona, M.T. Lopez-Lopez, M. Alaminos, V. Carriel, I.A. Rodriguez, *Front*
647 *Bioeng Biotechnol*, 8 (2020) 596.

648 [35] J. Chato-Astrain, C. Philips, F. Campos, D. Durand-Herrera, O.D. Garcia-Garcia, A.
649 Roosens, M. Alaminos, A. Campos, V. Carriel, *J Tissue Eng Regen Med*, 14 (2020) 789-806.

650 [36] V. Carriel, J. Garrido-Gomez, P. Hernandez-Cortes, I. Garzon, S. Garcia-Garcia, J.A.
651 Saez-Moreno, M. Del Carmen Sanchez-Quevedo, A. Campos, M. Alaminos, *J Neural Eng*, 10
652 (2013) 026022.

653 [37] A. Gloria, T. Russo, U. D'Amora, S. Zeppetelli, T. D'Alessandro, M. Sandri, M.
654 Banobre-Lopez, Y. Pineiro-Redondo, M. Uhlarz, A. Tampieri, J. Rivas, T. Herrmannsdorfer,
655 V.A. Dediu, L. Ambrosio, R. De Santis, *J R Soc Interface*, 10 (2013) 20120833.

656 [38] A.K. Gupta, M. Gupta, *Biomaterials*, 26 (2005) 3995-4021.

657 [39] M.T. Lopez-Lopez, A. Gomez-Ramirez, L. Rodriguez-Arco, J.D. Duran, L. Iskakova, A.
658 Zubarev, *Langmuir*, 28 (2012) 6232-6245.

659 [40] A. Tampieri, T. D'Alessandro, M. Sandri, S. Sprio, E. Landi, L. Bertinetti, S. Panseri, G.
660 Pepponi, J. Goettlicher, M. Banobre-Lopez, J. Rivas, *Acta Biomater*, 8 (2012) 843-851.

661 [41] A. Tampieri, E. Landi, F. Valentini, M. Sandri, T. D'Alessandro, V. Dediu, M. Marcacci,
662 *Nanotechnology*, 22 (2011) 015104.

663 [42] J. Li, Z. Yuan, H. Liu, J. Feng, Z. Chen, *J Nanobiotechnology*, 17 (2019) 124.

664 [43] R. Weissleder, D.D. Stark, B.L. Engelstad, B.R. Bacon, C.C. Compton, D.L. White, P.
665 Jacobs, J. Lewis, *AJR Am J Roentgenol*, 152 (1989) 167-173.

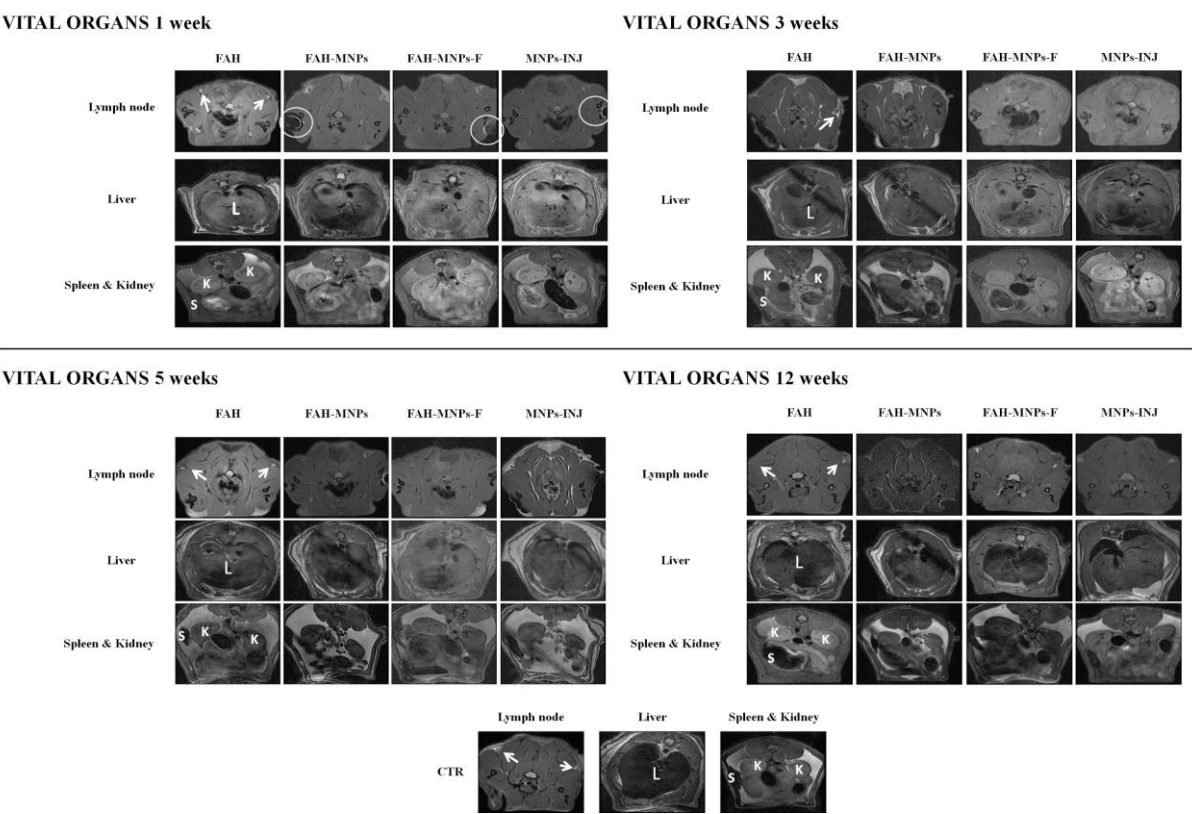
666 [44] C. Song, X. Meng, Y. Liu, A. Shen, C. Shao, K. Wang, H. Cheng, X. Fang, P. Wang, W.
667 Bu, *Biomaterials*, 230 (2020) 119631.

668 [45] L. Rico-Sanchez, I. Garzon, M. Gonzalez-Andrades, A. Ruiz-Garcia, M. Punzano, A.
669 Lizana-Moreno, J.I. Munoz-Avila, M.D.C. Sanchez-Quevedo, J. Martinez-Atienza, L. Lopez-
670 Navas, R. Sanchez-Pernaute, R.I. Oruezabal, S. Medialdea, M.D.C. Gonzalez-Gallardo, G.
671 Carmona, S. Sanbonmatsu-Gamez, M. Perez, P. Jimenez, N. Cuende, A. Campos, M.
672 Alaminos, *J Tissue Eng Regen Med*, 13 (2019) 2142-2154.

673 [46] E.A. Neuwelt, C.G. Varallyay, S. Manninger, D. Solymosi, M. Haluska, M.A. Hunt, G.
674 Nesbit, A. Stevens, M. Jerosch-Herold, P.M. Jacobs, J.M. Hoffman, *Neurosurgery*, 60 (2007)
675 601-611; discussion 611-602.

- [47] M. Wankhede, A. Bouras, M. Kaluzova, C.G. Hadjipanayis, *Expert Rev Clin Pharmacol*, 5 (2012) 173-186.
- [48] P. Lakhani, K.K. Dwivedi, N. Kumar, *J Mech Behav Biomed Mater*, 104 (2020) 103693.
- [49] C. Gila-Vilchez, M.C. Manas-Torres, R. Contreras-Montoya, M. Alaminos, J.D.G. Duran, L.A. de Cienfuegos, M.T. Lopez-Lopez, *Philos Trans A Math Phys Eng Sci*, 377 (2019) 20180217.
- [50] E. Teeman, C. Shasha, J.E. Evans, K.M. Krishnan, *Nanoscale*, 11 (2019) 7771-7780.
- [51] A.S. Zhang, C.A. Enns, *Hematology Am Soc Hematol Educ Program*, (2009) 207-214.
- [52] N. Dasgupta, S. Ranjan, C. Ramalingam, M. Gandhi, *3 Biotech*, 9 (2019) 125.
- [53] A. Isaacson, S. Swioklo, C.J. Connon, *Exp Eye Res*, 173 (2018) 188-193.
- [54] A. Sensini, C. Gualandi, A. Zucchelli, L.A. Boyle, A.P. Kao, G.C. Reilly, G. Tozzi, L. Cristofolini, M.L. Focarete, *Sci Rep*, 8 (2018) 17167.
- [55] J.P. Wu, T.B. Kirk, M.H. Zheng, *J Orthop Surg Res*, 3 (2008) 29.
- [56] P. Liu, J.Y. Zhu, B. Tang, Z.C. Hu, *J Microsc*, 270 (2018) 170-175.

707



708

709

710

711

712

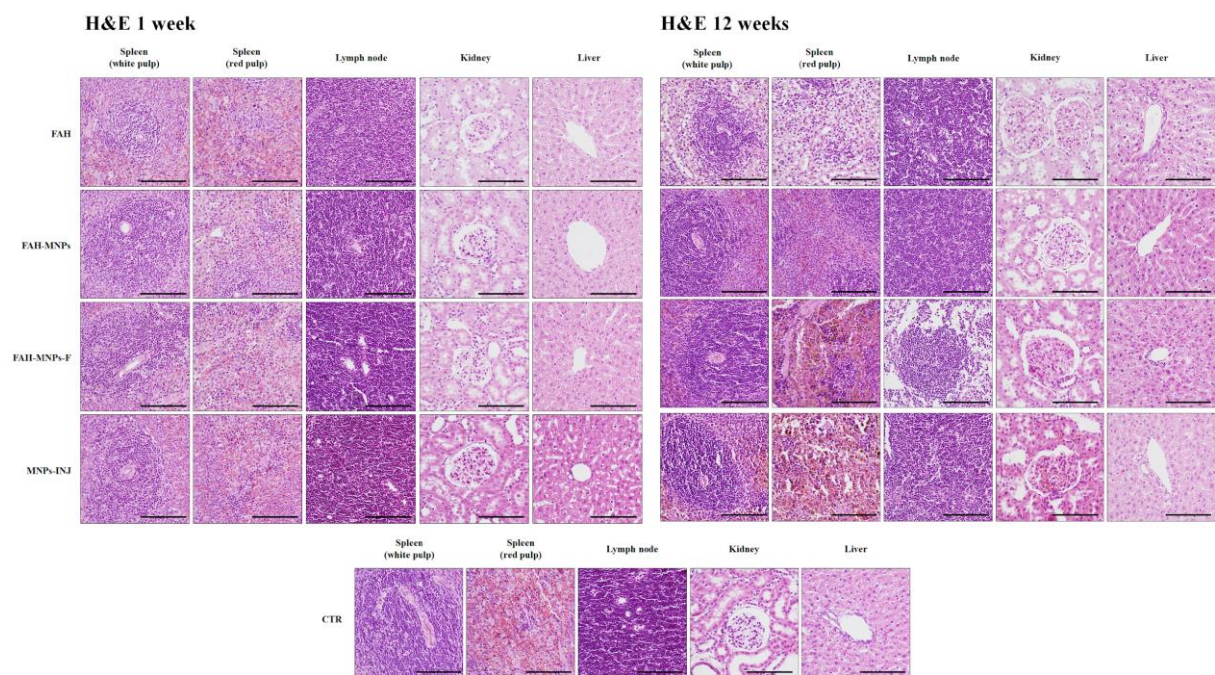
713

714

715

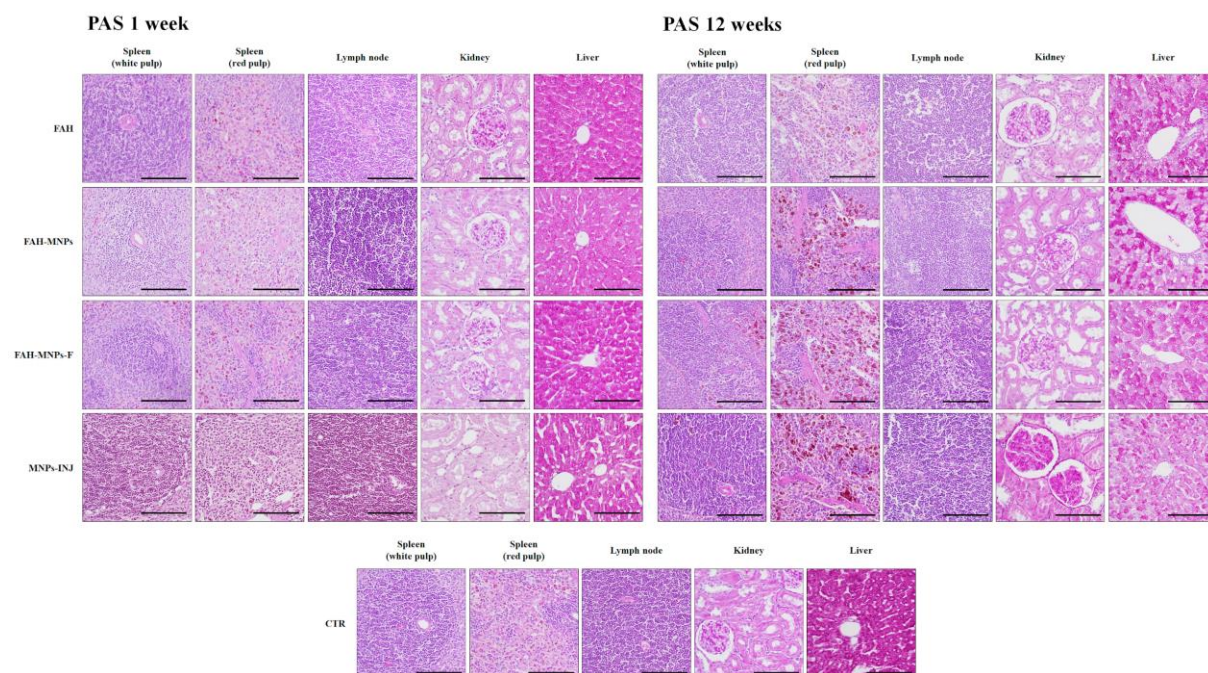
Supplementary Figure S1. MRI analysis of vital organs at each study time. FAH: fibrin-agarose hydrogels; FAH-MNPs: FAH containing MagNP-OH; FAH-MNPs-F: FAH containing MagNP-OH subjected to a magnetic field during gelation; MNPs-INJ: MNPs injected subcutaneously; CTR: control animals. White arrows: Lymph node; L: Liver; S: Spleen; K: Kidney.

716



717
718
719
720

Supplementary Figure S2. Histological analysis of four major distal organs using haematoxylin and eosin staining (H&E). FAH: fibrin-agarose hydrogels; FAH-MNPs: FAH containing MagNP-OH; FAH-MNPs-F: FAH containing MagNP-OH subjected to a magnetic field during gelation; MNPs-INJ: MNPs injected subcutaneously; CTR: control animals. Scale bar 100 μ m.



Supplementary Figure S3. Histochemical analysis of four major distal organs using the PAS method. FAH: fibrin-agarose hydrogels; FAH-MNPs: FAH containing MagNP-OH; FAH-MNPs-F: FAH containing MagNP-OH subjected to magnetic field during gelation; MNPs-INJ: MNPs injected subcutaneously; CTR: control animals. Scale bar 100 μ m.